**Geoscientific
Model Development
Discussions**

Simulating Southern Hemisphere extra-tropical climate variability with an idealized coupled atmosphere-ocean model

H. Kurzke[1,*], M. V. Kurgansky[2], K. Dethloff[1], D. Handorf[1], D. Olbers[3], C. Eden[4], and M. Sempf[5,**]

[1]Alfred Wegener Institute for Polar and Marine Research, Research Unit Potsdam, Potsdam, Germany
[2]A. M. Obukhov Institute of Atmospheric Physics, Russian Academy of Sciences, Moscow, Russia
[3]Alfred Wegener Institute for Polar and Marine Research, Bremerhaven, Germany
[4]Institute of Oceanography, University of Hamburg, Hamburg, Germany

Discussion Paper | Discussion Paper | Discussion Paper | Discussion Paper

GMDD

4, 1907–1940, 2011

Simulating Southern Hemisphere extra-tropical climate

H. Kurzke et al.

Title Page

Abstract | Introduction

Conclusions | References

Tables | Figures

◄ | ►

◄ | ►

Back | Close

Full Screen / Esc

Printer-friendly Version

Interactive Discussion

[5]SDA Software Design Ahnert GmbH, Berlin, Germany
[*]current address: Institute for Physics and Astronomy, Potsdam University, Potsdam, Germany
[**]formerly at: Max Planck Institute for Plasmaphysics, Muenchen-Garching, Germany

Correspondence to: K. Dethloff (klaus.dethloff@awi.de)

Abstract

The design and implementation of a simplified coupled atmosphere-ocean model over mid and high Southern Hemisphere latitudes are described. The development of the model is motivated by the clear indications of important low-frequency variability of ex-tratropical origin in atmosphere-only models and the crucial role of atmosphere-ocean interaction in altering and shaping the climate variability on decadal and multidecadal time-scales. The basic model consists of an idealized quasi-geostrophic model of Southern Hemisphere's wintertime atmospheric circulation coupled to a general ocean circulation model with simplified physics. Model spin-up is described, some basic descriptors of the model climatology are discussed, and it is argued that the model exhibits skill in reproducing essential features of decadal and multi-decadal climate variability in the extratropical Southern Hemisphere. Notably, 1000 yr long coupled model simulations reveal sea surface temperature fluctuations on the timescale of several decades in the Antarctic Circumpolar Current region.

1 Introduction

Understanding natural variability on interannual-to-multidecadal time scales is an important and longstanding problem in climate dynamics. In this study we will be focusing on the interannual, decadal and multidecadal variability in the extra-tropical Southern Hemisphere (SH) and on the relative role of the atmosphere and the ocean in its explanation. The principal mode of the aforementioned variability, which is not directly related to El Niño-Southern Oscillation (ENSO), has been named the High Latitude Mode (HLM) (Kidson, 1999, and references therein), or the Southern Annular Mode (SAM), or the Antarctic Oscillation (AAO) (Thompson and Wallace, 2000). The AAO is a zonally symmetric pattern in the sea level pressure field with opposite signs between the Antarctica and midlatitudes, which originates in the atmosphere-only dynamics. However, the atmosphere-ocean coupling over the largely aquatic SH undoubtedly plays an important role in shaping the leading modes of extratropical low-frequency climate

variability, but the operating mechanisms remain somewhat obscure. For example, the observational studies have suggested the existence of a wavenumber-2 pattern with a 4-yr period at the ocean–atmosphere interface of the Southern Ocean and it was hypothesized that this Antarctic Circumpolar Wave (ACW) represents a coupled atmosphere–ocean mode (White and Peterson, 1996). Of course, spatial and temporal sparsity of observations is not unique to the Southern Ocean, but it is more conspicuous there than elsewhere. Hence, coupled models of the oceanic and atmospheric circulation are indispensable for the study of the ACW and other leading modes of the SH low-frequency climate variability to facilitate greater understanding (cf., Marsland et al., 2003).

An important aspect of the discussed problem concerns the Antarctic Circumpolar Current (ACC) transport. Olbers and Lettmann (2007) have applied a global ocean circulation model with simplified physics (the barotropic-baroclinic-interaction model BARBI of Olbers and Eden, 2003) and, in one of their main experiments, forced BARBI by an artificial wind stress constructed from the first three empirical orthogonal functions (EOFs) of the National Center for Environmental Prediction/National Center for Atmospheric Research (NCEP-NCAR) combined with a temporal variability according to an autoregressive process. By design, BARBI can be forced by a surface wind stress and a surface source of the baroclinic potential energy, but Olbers and Lettmann (2007) set the latter term to zero and a purely wind-driven variability of the Southern Ocean was studied. A 1800 yr BARBI run with this SAM-type forcing showed that "the Southern Mode" of variability (cf. Hughes et al., 1999) with coherence between ACC transport, Southern Ocean wind-stress and bottom pressure extends to periods well above decadal. For these periods, baroclinic processes come into play and the baroclinic potential energy, as manifestation of the baroclinic pressure, takes control of the ACC transport. In these circumstances BARBI behaves similar to Hasselmann's (1976) stochastic climate model, with the ACC transport as the fast variable, the baroclinic pressure gradient across Drake Passage as the slow variable, and the wind stress as red noise forcing (the latter in contrast to the classical stochastic model).

Simulating Southern Hemisphere extra-tropical climate

H. Kurzke et al.

This study aims at the work of Olbers and Lettmann (2007) by coupling the oceanic BARBI to an idealized three-level quasi-geostrophic model of atmospheric circulation over the SH, which has earlier been used in Weisheimer et al. (2003) for an assessment of the influence of the horizontal resolution on decadal-scale variability, in Sempf et al. (2005) for an idealized modelling of the Northern Annular Mode, and in Sempf et al. (2007a, b) for analyses of circulation regimes emerging in baroclinic atmospheric models. This idealized atmospheric model has been adapted to the SH. In the Northern Hemisphere (NH), the absence of an atmospheric model is circumvented by incorporating the annual mean wind forcing taken from the European Centre for Medium Weather Forecast (ECMWF) reanalysis data. The used approach does not follow a more conventional practice of coupling a global atmosphere model to a global ocean model but is more reminiscent of, e.g., the work by Mikolajewicz et al. (2005) who coupled the global ocean model to the regional atmospheric model over the Arctic, forced with reanalysis data. Our model occupies an intermediate position in the hierarchical set of models ranging from comprehensive state-of-the-art coupled global circulation models (coupled GCMs, or CGCMs) to very idealized coupled models, which have omitted a fully dynamical atmospheric component, including ocean models coupled to energy-balance atmospheric models (see, Farneti and Vallis, 2011 and references therein). Compared to the latter models, we opt for a simplified but dynamically more solid framework via the use of the quasi-geostrophic atmospheric component, similar in this respect to, e.g., Opsteegh et al. (1998), Haarsma et al. (2000), Hogg et al. (2003), and Hogg and Blundel (2006).

In this idealized modeling set-up, we omit dynamical interaction between the atmosphere and the ocean in the tropics, notably the ENSO phenomenon, and focus exclusively on extratropical sources of the climate variability over mid- and high SH latitudes. We also discard the cross-equatorial interaction between the hemispheric atmospheres. In the model this interaction occurs indirectly, via the oceanic global circulation. There are other inherent simplifications and idealizations in the model, described in Sect. 2. However, going into too many details and trying to maximize the

"model realism" may appear not the best strategy. Rather, considering our model as a conceptual tool to better understand the role of the extratropical atmosphere-ocean coupling in the SH in producing and modifying interannual-to-multidecadal climate variability is the primary goal of this study.

5   This paper is organized as follows. In Sect. 2 we explain the constructed coupled atmosphere-ocean model. Section 3 describes the model set-up and presents the results of 1000 yr model simulations. The obtained results are discussed and conclusions are drawn in Sect. 4. In Appendix A the used version of oceanic model BARBI is described in more detail. In Appendix B we show the details of atmosphere-ocean

10   thermal coupling and relate the baroclinic potential energy in BARBI to the sea surface temperature (SST).

2   Model description

The coupled atmosphere-ocean model consists of three modules: for the atmosphere, the ocean and the coupling procedure, respectively.

15   ## 2.1   Atmospheric module

The dynamic core of the atmospheric module is the quasi-geostrophic potential vorticity equation. It is a hemispheric 3-layer model with a T21 spectral resolution. The spectral interaction coefficients are found by transformation from the spectral space onto a grid with 64 points in the zonal direction, which corresponds to a resolution of 5.625° in

20   longitude, and with 32 points in the meridional direction (the Gaussian latitudes). The latter points are symmetric with respect to the equator, i.e. there are 16 points in the SH but the distance between them slightly varies according to the relative weight of different Gaussian latitudes. It is a dry model. That is, no clouds, no precipitation (rainfall) and no latent heat are taken into account explicitly. Non-zonal components of extra-

25   tropical thermal forcing (radiative equilibrium temperature fields) have been adjusted

in a way that, on the time mean, realistic patterns of non-zonal extra-tropical diabatic heating are acting in the model. The zonal components of the radiative equilibrium temperature fields and the surface forcing, which acts as a substitute for the absent baroclinicity within the lowermost layer and helps to enforce low-level westerlies, have been tuned to produce a zonal climatology as realistic as possible. The adjustments of forcing are made by an automatic iterative procedure. The atmospheric module developed in Weisheimer et al. (2003) and Sempf et al. (2005, 2007a, b) and adapted to the SH is abbreviated as GS3LM, hereafter.

2.2 Oceanic module

The oceanic module uses vertically integrated dynamical equations in terms of the streamfunction of volume transport, Ψ, the baroclinic potential energy of individual water columns scaled by a constant reference seawater density, E, and a baroclinic velocity moment, $\boldsymbol{u}^*$ (see, Appendix A). This is a simplified version of BARBI (Olbers and Eden, 2003; Olbers et al., 2007; Olbers and Lettmann, 2007) which accounts for a joint effect of baroclinicity and bottom relief (JEBAR, Sarkisyan and Ivanov, 1971). JEBAR is a prominent source of vorticity in addition to the windstress curl and flow across the geostrophic contours in a vertically averaged view of the flow. The used oceanic module has 91 grid points in the zonal direction and 75 grid points in the meridional direction. It corresponds to a resolution of $4° \times 2°$ longitude/latitude. There is a grid asymmetry with respect to the equator: an integration area extends from 77° S to 71° N. The lateral ocean boundary conditions assume the no-slip condition $\mathbf{u}=0$ (see notations in Appendix A) and vanishing fluxes of potential energy.

2.3 Coupling module

The design and numerical implementation of the coupling module is based on a beta version of Modular Ocean Model MOM2 (Version 2.0), as "a stepping stone" to MOM3 (Pacanowski, ed., 1996; Pacanowski and Griffies, 2000). The coupling methodology,

Title Page

Abstract | Introduction

Conclusions | References

Tables | Figures

|◄ | ►|

◄ | ►

Back | Close

Full Screen / Esc

Printer-friendly Version

Interactive Discussion

most "interface" files and code fragments come from MOM2, but several modifications have been made.

2.4 Atmospheric GS3LM versus oceanic BARBI

GS3LM simulates the quasi-geostrophic evolution of SH atmospheric flow streamfunctions at the three vertical levels 167, 500, and 833 hPa under perpetual SH winter conditions. Southern Hemisphere's T21 topography (Fig. 1a) acts as orographic forcing. Diabatic heating is established by thermal relaxation towards predefined radiative equilibrium temperature fields at the auxiliary model pressure levels 333 and 667 hPa. The relaxation timescale is 22.7 days. Slightly differently to the NH (Sempf et al., 2005), the temperature lapse rate is fixed to $2.9\,\mathrm{K\,km^{-1}}$ at 333 hPa and $6.5\,\mathrm{K\,km^{-1}}$ at 667 hPa. The relaxation time of Ekman friction equals to 2.2 days. Other parameter settings are the same as in Sempf et al. (2005). The cited paper describes an automatic iterative procedure of the atmospheric model pre-tuning before coupling to the ocean model. First, the model's time-mean wind profiles are compared with and then are iteratively tuned towards observed SH wintertime zonal winds taken from NCEP-NCAR reanalysis data. Second, within the same iterative procedure the model's time-mean non-zonal diabatic heating is compared with and then is tuned towards the non-zonal part of SH wintertime heating fields at 300 and 700 hPa, derived from observations by Nigam et al. (2000). The latter fields have been attenuated near the equator and are shown in Fig. 1b–c. Thus tuned, GS3LM exhibits a pronounced internal "ultra-low-frequency" variability that manifests itself in various atmospheric fields, similar in this respect to the pioneering simulations by James and James (1992); see a recent discussion of the latter work in Vallis (2010).

BARBI accounts for the JEBAR effect in the vertically averaged vorticity equation without any depth scaling as, e.g., required in quasi-geostrophic models. Considering the JEBAR-term in the vorticity equation necessitates a prognostic equation for the baroclinic potential energy E. When the baroclinic flow component is accounted for, the governing equations cannot be written in a closed form but give rise to an infinite

set of equations for the moments of the density field, with E as the first moment, and also for the moments of the baroclinic velocity.

In this work, a simple truncation and subsequent closure of this infinite set of equations is made after Olbers and Eden (2003). As in Olbers and Eden (2003), an account for non-linearity is made in the thermohaline balance equation only. Advection of momentum in the momentum balance equation is neglected since the emphasis is placed mainly on large-scale flows (Olbers and Eden, 2003). The ocean bottom topography is shown in Fig. 2. The parameters of the oceanic module were chosen so that the transport through Drake Passage was within the range 100–150 Sv ($1\,\text{Sv} = 10^6\,\text{m}^3\,\text{s}^{-1}$). This comparison is especially useful because there are good oceanographic measurements for Drake Passage, in contrast to the rest of Southern Ocean. Based on various previous studies, Cunningham et al. (2003) present the mean estimate 137 ± 8 Sv.

Detailed sensitivity analysis and discussion of the parameter setting can be found in Olbers at el. (2007) and Olbers and Lettmann (2007). For a time-constant wind forcing BARBI reaches a stationary state after its spin-up (Olbers et al., 2007) but for variable winds shows pronounced time-variability as a quasi-linear response to the non-stationary forcing (Olbers and Lettmann, 2007).

2.5 Atmosphere-ocean coupling

The two-way coupling between GS3LM and BARBI is organized as follows. The ocean circulation is driven by the atmospheric wind, where the surface wind stress is described by a linearized bulk formula

$$\boldsymbol{\tau} = c_D \rho_a |\boldsymbol{V}_s| \boldsymbol{v}_s. \tag{1}$$

Here, $c_D = 0.013$ is the drag coefficient, $\rho_a = 1.25\,\text{kgm}^{-3}$ is the standard surface air density, and $|\boldsymbol{V}_s| = \sqrt{\left(\frac{\partial \psi_s}{\partial x}\right)^2 + \left(\frac{\partial \psi_s}{\partial y}\right)^2}$ is the wind speed at the 10 m height. The 10-m wind velocity vector reads $\boldsymbol{v}_s = \boldsymbol{k} \times \nabla \psi_s$, where **k** is the unit vector directed upward, and

the streamfunction ψ_s is taken proportional to that at 833 hPa level, with the reduction coefficient $k = 0.7$. In the NH the oceanic model is forced with interpolated annual mean (over 1986–1988) wind stress data from ECMWF analysis (Barnier et al., 1995) (surface density forcing is omitted). The backward influence of the ocean circulation on the atmosphere is achieved through the SST-related heat fluxes. They are described by a linearized bulk formula

$$H = c_H \rho_a c_p |\boldsymbol{V}_s|(\text{SST} - \text{SAT}) \qquad (2)$$

with the heat exchange coefficient $c_H = c_D$ and $|\boldsymbol{V}_s| = 5\,\text{ms}^{-1}$ is the standard wind speed at the 10 m height. In this formula, $c_p = 1004\,\text{m}^2\,\text{s}^{-2}\,\text{K}^{-1}$ is the specific heat at constant pressure, SAT abbreviates the surface air temperature; other notations are as in Eq. (1). The direct thermal forcing of the oceanic circulation is omitted (see also Appendix B). The use of E as a prognostic variable in BARBI leads to a difficulty: the atmosphere is sensitive to the seawater temperature T (specifically to SST) but indifferent to the salinity S and to the seawater density (and so E-values) per se. A problem arises to extract information on oceanographic variables, T and S, that is contained in E and translate it into the SST-terms. An important simplification permissible for SH oceans will be to assume that the basin-averaged vertical density stratification is mainly explained by S-values, whereas the density deviations specifying E distribution are mainly determined by T-variations (e.g., Falcini et al., 2009).

In the thermally balanced model a systematic heat exchange between the atmosphere and the ocean is not allowed, also because all other constitutive elements of the oceanic heat balance (radiative forcing, etc.) are not considered in this simplified framework. It means that the basin-averaged SST value should coincide with the analogously averaged SAT-value, and moreover cannot vary in time. The latter is due to intrinsic limitations imposed by the quasi-geostrophic nature of GS3LM (see also Appendix B); however, this constraint is not seen as a very restrictive one for the largely oceanic ($\approx 80\,\%$ by area) SH. Therefore, the deviations of SST and SAT from this common time-constant value (hereafter, these temperature deviations are denoted

as SST′ and SAT′) appear in Eq. (2). The details of E to SST′ conversion are given in Appendix B, see especially Eq. (B1).

3 Model results

3.1 Model experiment

Initially, a 1000-yr spin-up run of BARBI from the state of rest without coupling to the atmospheric GS3LM was carried out. It was found that the oceanic circulation after 200 yr reaches a quasi-stationary state with $\approx$ 140 Sv (Fig. 3a–d). Dark circles with numbers 1, 2, 3 in Fig. 3a mark three grid points across Drake Passage for which a temporal behavior of the streamfunction Ψ is demonstrated in Fig. 3b–d. This stationary state has been used as an initial state for the further model integration. Afterwards, the already pre-tuned by the aforementioned automatic iterative procedure GS3LM was during 8000 days additionally tuned by the same procedure towards NCEP-NCAR reanalysis data, since the forcing terms describing the atmosphere-ocean heat exchange are now taken into account (see, Appendix B) but SST′-values in them are temporarily set to zero. Finally, using the fine-tuned atmospheric module and a steady-state oceanic circulation, as an initial state, the fully coupled atmosphere-ocean model is run over 1000 yr under perpetual SH winter conditions.

3.2 Model climatology

Figure 4 shows the time-mean zonal wind profile over 1000 yr of integration of the coupled model versus zonal wind profiles inferred from austral wintertime NCEP-NCAR reanalysis data. The latter have been computed after averaging the reanalysis data over three vertical atmospheric layers of approximately equal mass, instead of using individual pressure level data. It was done to capture the contribution of the stratospheric polar vortex. As visible in Fig. 4, the agreement between the modeled and the

observed wind profiles is fairly good, though the tuning procedure applied to the SH (both for the atmosphere-only and the coupled atmosphere-ocean model) encounters more difficulties compared to the NH, where such an agreement for the atmosphere-only model is almost perfect (Sempf et al., 2005). The wind speed maximum situated at

5 about 30° S at the middle and upper level corresponds to the subtropical jet (STJ). The second maximum in the upper level wind profile is due to the polar front jet (PFJ) across the South Pacific east of Australia during the austral winter. Together, STG and PFG compose a "split jet" ("double jet") structure over the South Pacific (e.g., Bals-Elsholz et al., 2001), which manifests itself in zonal-averaged wind profiles.

10 The atmospheric module exhibits skill in reproducing the polar vortex. This pattern is very persistent through all 1000 yr of model integration and clearly is exhibited in 1000-yr averages (not shown), but the corresponding standard deviation as compared to the observations is rather small (not shown).

Figure 5 repeats Fig. 3 but for the last 10 yr time slice of the coupled model run. On

15 time-average, there is a moderate, by ≈15–20 %, reduction in Ψ-values in Drake Passage, compared to an uncoupled spin-up run (Fig. 3), but these values remain within the range of experimentally observed values (see Sect. 2.4). Figure 5b–d demonstrate temporal behavior of the streamfunction Ψ for three grid points across Drake Passage, shown in Fig. 3a. Note that Ψ-values are monotonic increasing southward, consis-

20 tently with the westerly flow of ACC. Figure 9a presents 1000 yr mean climatology of the baroclinic potential energy E, whereas the field of SST-deviations from the basin-average value (SST$'$) is shown in Fig. 9b. There is a high correlation between E and SST$'$ but the impact of variable oceanic depth h, see Eq. (B1), is clearly visible, too.

3.3 Model variability

25 The time-variance of Ψ is about 20 Sv in Drake Passage (Fig. 5b–d). In BARBI-only runs this variance vanishes for a time-constant wind forcing (Fig. 3) and therefore quantifies the coupling of the ocean model to its chaotically behaving atmospheric counterpart. There is an apparent correlation between fluctuating Ψ-values in Fig. 5c–d, which

H. Kurzke et al.

means that, to a large extent, the westerly flow in the southern part of Drake Passage (between 61° S and 63° S) does not experience strong time-variations but demonstrates a gradual, though not very much significant, positive climatic trend. It hints on a very slow spinning-up of the Southern Ocean circulation, probably due to minor imbalances in the coupled model. Figure 5b-d shows also an initial transient in the first 30 yr as a result of coupling. The major part of transport variability through Drake Passage is explained by the fluctuating flow through its northern part between 61° S and the southernmost part of South America (Tierra del Fuego). In our model, this northern part of the flow explains about 50 % of the total transport through Drake Passage.

What is the physics of model variability seen in Fig. 5? Does it originate in the atmospheric dynamics and the ocean redistributes or integrates it? The leading mode of low-frequency variability in the SH troposphere is AAO/SAM (e.g., Thompson and Wallace, 2000) and the AAO index is defined as the leading principal component of the 850-hPa geopotential height anomalies south of 20° S (Thompson and Wallace, 2000). In the coupled model simulations, the AAO pattern is successfully reproduced versus observations at 833 hPa atmospheric model level (Fig. 6b–c); the corresponding first EOF for a 1000 yr GS3LM-only run is shown in Fig. 6a. The priority is set in this work to BARBI, which has been proven efficient in simulating the predominantly wind-driven Southern Ocean circulation. Besides, the lower-level-only information from GS3LM is used to compute the acting wind stress. Therefore, the AAO as the leading mode of atmosphere-ocean dynamic interaction on long time scales and at mid- and high SH latitudes is reproduced satisfactorily, which gives an incentive to use the constructed coupled model in this study.

In our experiment, BARBI is forced by a chaotically behaving GS3LM with most effect on synoptic time-scale (Figs. 7, 8). On this time-scale, the fluctuating wind stress drives the fast barotropic BARBI-subsystem, where the transport streamfunction Ψ serves as the fast variable (Fig. 5b–c). The slow baroclinic BARBI-subsystem, quantified by the baroclinic potential energy E and JEBAR-term, effectively integrates the fast "stochastic" forcing implemented by the wind stress and the barotropic pumping action

of the mean stratification (the first term on right-hand-side of (A2)), which is displayed in Fig. 10. On these long time scales the ocean imposes a feedback on the atmospheric circulation, through SST-variations which are inferred from the slow E-variable that dominates the low-frequency variability in BARBI. The ocean in BARBI acts as a quasi-linear capacitor that integrates and at long time-scales non-linearly transforms, due to a non-linearity inherent in Eq. (A2), the chaotic signal from the atmosphere on synoptic-to-decadal time-scales. At long time-scales, the ocean is also directly forced by the wind stress, because the spectra of atmospheric fluctuations extend to very low frequencies. The first and the second EOF for SST′ over the entire SH are shown in Fig. 10a–b. It is visible that these leading variability patterns are dominated by processes in the Pacific. To enhance alternative variability patterns, which otherwise remain obscure within the hemispheric approach, the SH ocean was subdivided into four domains, the Southern Pacific, the Southern Atlantic, the Southern Indian Ocean and the ACC (the Southern Ocean), and the EOF analysis has been applied to each of them. Here, we focus mainly on the ACC (a ring-like domain between 60° and 70° S) show the corresponding first and second EOF (Fig. 10c–d). For comparison, the same EOFs but for the Southern Pacific (152° E–90° W, 20°–60° S) are shown in Fig. 10e–f and resemble those ones in Fig. 10a–b. So, the power spectrum of the first principal component (PC1) for the Southern Pacific, showing the dominance of variability on interannual time-scale and also a significant peak at about 15 yr (Fig. 11d), is characteristic for the entire SH ocean, and it makes obscure a remarkable multi-decadal and even centennial variability in the ACC, see Fig. 11b. The wavelet spectra for the ACC supporting these findings are shown in Fig. 12b–c.

4 Conclusions

A new simplified coupled atmosphere-ocean model with inherent non-linear dynamics has been developed aiming at the examination of decadal and multi-decadal climate variability over mid and high SH latitudes, arising in the model, and of the role of atmosphere-ocean interaction in altering and shaping it.

By coupling the hemispheric quasi-geostrophic atmospheric model with horizontal resolution T21 to a global ocean circulation model with simplified physics (the barotropic-baroclinic-interaction model BARBI), it was possible to realistically reproduce large-scale extratropical atmospheric processes in the Southern Hemisphere and also the transport properties of the Southern Ocean circulation in accord with the essential features of observations.

Due to the coupling, there is significant oceanic low-frequency variability apparent in the SST anomaly (SST′) time-variations and demonstrated in Figs. 10–12. The first EOF of the simulated SST′ shows a similarity with observed patterns (e.g., Doney et al., 2003, 2007). The spectral analysis of the temporal evolution of the dominant variability patterns makes it clear that while the power spectra for the atmosphere-only model are more white (Fig. 7a), the power and wavelet spectra of atmospheric variables for the coupled model demonstrate more apparent red behavior (Figs. 7b, 11a and 12a). Crucial to thus enhanced redness is the parameterization of interaction between the atmosphere and the ocean. Theoretically, the effect of reddening is described, e.g., by Vallis (2010). The ocean acts as an integrator of variability on short time scales, which leads to shifting of the maxima in the atmospheric spectra to low frequencies. Following Hasselmann (1976), Vallis (2010) characterizes the reddening of the atmospheric variability by the ocean as the null hypothesis for climate variability. The effect of reddening is obviously present in our coupled model, as follows from Figs. 7a, b, 11a and 12a.

It was also detected that significant spectral peaks are observed in the power spectra of oceanic variables, which coincide with the dominant frequencies in the power spectra of the atmospheric variables (cf. Figs. 11a, b, d). Particularly noteworthy are the time periods from about 15 to 35 yr with a maximum at about 20–25 yr. Also, Farneti and Vallis (2009) reported an oscillation at about 20 yr. However, these authors used a three-dimensional atmosphere-ocean-land-ice global circulation model of intermediate complexity and associate the oscillation with the meridional overturning circulation (MOC). The MOC in BARBI is poorly reproduced, since only the first density moment

Full Screen / Esc

Printer-friendly Version

Interactive Discussion

(baroclinic potential energy) is retained and so the vertical resolution is relatively low. In addition, our calculated power spectra show significant peaks at time-periods around 50 and 90 yr. For globally averaged boreal winter mean SST, the peak at approximately a 64 yr period was also found in numerical simulations by Opsteegh et al. (1998) who associated the peak with large scale variability in the Southern Ocean. Time-periods of 15–30 and 65–70 yr are indeed observed in the real ocean; some evidence comes from the frequency analysis of proxy data (Mantua and Hare, 2002).

In this study it was assumed that the momentum and heat exchange coefficients (c_D and c_H) in Eqs. (1) and (2) are basically the same. However, this is valid only for a certain range of c_D-values and an inequality $c_D \neq c_H$ (see e.g. Liu et al., 1979; Gill, 1982) could be accounted for in the model, in an attempt to improve its "realism". It is also possible to analyze circulation regimes, or preferred states of the atmospheric circulation occurring on large and planetary scales, which emerge in the model, as was done in Sempf et al. (2007a, b) for the atmosphere-only model applied to the Northern Hemisphere. Further experimentation with the model is challenging, especially as far as it regards the circulation regime behavior dependent on various model parameters, including the coupling constants c_D and c_H. The horizontal resolution of the atmospheric and oceanic modules should be increased to be able to simulate more realistic wind patterns and finer scale ocean circulation systems such as Humboldt Current and the overall current system in the southeast Pacific (cf. Dávila and Figueroa, 2001). Increasing vertical resolution in the atmospheric module and accounting for higher density moments in the oceanic module would also increase the realism of the simulations with the coupled model.

The atmosphere-ocean system constitutes the fundamental subsystem of the Earth climate system, and this offers an opportunity of basic research of the climate variability with the use of coupled atmosphere-ocean models. Among these models our model fills the gap between the models of so-called intermediate complexity but with GCM-flavor (e.g., Farneti and Vallis, 2009a) and simplified low-order box climate models (e.g., Roebber, 1995). The results of the current study emerge from a generally

time-consuming setup and pre-tuning of the atmospheric and oceanic modules, which constitute our coupled model. They are in any case promising and helping better understand the internal climate variability of the atmosphere-ocean system.

Appendix A

BARBI model

BARBI can be summarized by the set of equations (cf. Olbers and Eden, 2003):

$$\frac{\partial}{\partial t}\nabla\cdot\left(\frac{1}{h}\nabla\Psi\right) + J\left(\Psi,\frac{f}{h}\right) = J\left(E,\frac{1}{h}\right) + A_h\nabla\cdot\left(\frac{1}{h}\nabla\cdot\nabla^2_\otimes\Psi\right) + \frac{c_D\rho_a|\mathbf{V}_s|}{\rho_0}\nabla\cdot\left(\frac{1}{h}\nabla\psi_s\right), \quad (A1)$$

$$\frac{\partial E}{\partial t} + hJ\left(\Psi,\frac{E}{h^2}\right) = \frac{N^2}{3}J\left(\Psi,\frac{h^2}{2}\right) + \frac{N^2}{3}\nabla\cdot\mathbf{u}^* + K_h\nabla^2 E - \mu E, \quad (A2)$$

$$\frac{\partial}{\partial t}\mathbf{u}^* + f\,\mathbf{k}\times\mathbf{u}^* = -\frac{1}{3}\left(\nabla E^* - h^2\nabla E\right) + A_h\nabla^2\mathbf{u}^* - \frac{h^2}{3}\frac{c_D\rho_a|\mathbf{V}_s|}{\rho_0}(\mathbf{k}\times\nabla\psi_s). \quad (A3)$$

Here, h is the ocean depth, $E = \int_{-h}^{0} g\left(\rho/\rho_0\right) z\,dz$ is the potential energy referred to the sea surface level $z = 0$ and scaled by a constant reference density $\rho_0 = 1035\,\mathrm{kg\,m^{-3}}$; ρ is the density deviation from a mean background profile of density, g is the acceleration due to gravity and z-axis is directed upward. Mean background stratification is described by the Brunt-Väisälä frequency N. This is taken as being constant in this study and we use $N = 0.0026\,\mathrm{s^{-1}}$. In Eq. (A1), Ψ is the streamfunction of the barotropic flux velocity $\mathbf{U} = \int_{-h}^{0}\mathbf{u}\,dz$, where $\mathbf{u}$ is the (total) horizontal velocity; ∇ is the horizontal Nabla-operator, $\nabla^2_\otimes \equiv h\nabla\cdot\left(h^{-1}\nabla\right)$ is similar to the Laplacian ∇^2 but modified by the depth h in order to ensure positive definiteness of the viscous dissipation function; J denotes the Jacobian and f is the Coriolis parameter. Notations in the two

last terms in Eqs. (A1) and (A3), which are pertinent to the atmosphere-ocean inter-
action, are explained in the main text. The baroclinic velocity moment in Eqs. (A2)
and (A3) is defined by $\boldsymbol{u}^* = \int_{-h}^{0}(\boldsymbol{u} - \boldsymbol{U}/h)\,z^2\,dz$. To close Eqs. (A1)–(A3) it is used
that $E^* \equiv \int_{-h}^{0} g\left(\rho/\rho_0\right)z^3\,dz = \gamma\,h^2 E, \gamma = 1 - 6/\pi^2 \approx 0.3921$, which ensures an accurate
description of large-scale wave propagation in BARBI (Olbers and Eden, 2003). Co-
efficients $A_h = 20\,000\,\mathrm{m^2\,s^{-1}}$ and $K_h = 1000\,\mathrm{m^2\,s^{-1}}$ stand for a large-scale momentum
diffusivity and a turbulent heat (salt) diffusivity, respectively, based on the isopycnal
parameterization of meso-scale oceanic eddy effects by Gent and McWilliams (1990).
The dissipation coefficient of E is $\mu = 1.5 \times 10^{-10}\mathrm{s^{-1}}$ ($\mu^{-1} \approx 222\,\mathrm{yr}$).

Appendix B

Thermal coupling

The thermal coupling is applied to the atmosphere only. As follows from Eq. (2) and
discussion in Sect. 2.5, it is described with a linear forcing term proportional to SST′−
SAT′. By the hydrostatic law and for a standard temperature lapse rate, SAT′ is related
to the air temperature deviations from corresponding ocean basin-averaged values at
the auxiliary model levels 333 and 667 hPa: SAT′ $\approx 1.080\,T'_{333} \approx 1.234\,T'_{667}$ (for the
same longitude and latitude). It is further used that two thirds of the incoming heat is
spent on warming of the lower half of the atmosphere (mean level 667 hPa), and the
remaining one third goes to its upper half (mean level 333 hPa). In the prognostic equa-
tions for T''_{667} and T''_{333} (double primes denote deviations from hemisphere-averaged
values; see more in Weisheimer at al., 2003) it corresponds to an additional linear
forcing term with a relaxation time-scale of 20 and 35 days, correspondingly. The forc-
ing is applied to those grid points of the atmospheric model which are above ocean
grid points. Otherwise, it is set to zero. A systematic error, arising from a difference be-
tween the hemispheric-wide and the ocean-basin-wide average (in general, $T''_{667} \neq T'_{667}$,

Full Screen / Esc

Printer-friendly Version

Interactive Discussion

$T''_{333} \neq T'_{333}$), see also Sect. 2.5, is compensated by the applied fine-tuning of GS3LM during the 8000 day period; see Sect. 3.1.

To parameterize SST$'$, we use the formula

$$\mathrm{SS}T' \approx \frac{5.6E}{\alpha\,g\,h^2} + \frac{\beta S'}{\alpha}. \tag{B1}$$

Here α is the constant coefficient of seawater thermal expansion, β is the constant coefficient of seawater haline contraction, and S' is the deviation of near surface salinity from its basin-averaged value; other notations see in Appendix A. Equation (B1) stems from an assumption of the quadratic dependence on depth of the seawater density and of vanishing of the vertical density gradient at the sea bottom. Substituting these parabolic density profiles into E and $E^* \approx 0.3921\,h^2E$ (see, Appendix A) leads to a set of two equations to determine the surface density anomaly for a given E-value. A positive (negative) anomaly of E recasts in terms of a negative (positive) surface density anomaly, because E is referred to the level $z = 0$ and the sea depth z is ascribed negative values. Afterwards a linear equation of state for seawater is used to obtain Eq. (B1). Alternative parameterizations of the vertical density profile lead essentially to the same formula (B1) but with somewhat differing coefficients before E. However, keeping in mind all schematics of our coupled model, Eq. (B1) is used in the study. It is also used that the impact of salinity on the water density is generally of opposite sign to that of the temperature, and in the Southern Ocean these two effects hold in proportion 1:3 or even 1:5 (Levitus and Boyer, 1994). In a practical realization of the model, the second right-hand side term in Eq. (B1) is omitted, but instead a reduction factor, 0.7, is introduced before α in the denominator of the first right-hand-side term in this equation.

Simulating Southern Hemisphere extra-tropical climate

H. Kurzke et al.

Full Screen / Esc

Printer-friendly Version

Interactive Discussion

References

Bals-Elsholz, T. M., E. H. Atallah, L. F. Bosart, T. A. Wasula, M. J. Cempa, and A. R. Lupo: The Wintertime Southern Hemisphere Split Jet: Structure, Variability, and Evolution, J. Climate, 14(21), 4191–4215, 2001.

5 Barnier, B., Siefridt, L., and Marchesiello, P.: Thermal forcing for a global ocean circulation using a three year climatology of ECMWF analysis, J. Mar. Syst., 6, 363–380, 1995.

Cunningham, S. A., Alderson, S. G., King, B. A., and Brandon, M. A.: Transport and variability of the Antarctic Circumpolar Current in Drake Passage, J. Geophys. Res., 108(C5), 8084, 2003.

10 Dávila, P. M. and Figueroa, D.: Comparison of the analysed surface winds from ECMWF and NCEP with observable data, over the southeastern Pacific (35° S–62° S, 70° W–90° W), Australian Meteorological Magazine, 50(4), 279–293, 2001.

Doney, S. C., Yeager, S., Danabasoglu, G., Large, W. G., and McWilliams, J. C.: Modeling global oceanic inter-annual variability (1958–1997): Simulation design and model-data evaluation. NCAR Technical Note, National Center for Atmospheric Research, Boulder, Colorado (NCAR/TN-452+STR), 2003.

Doney, S. C., Yeager, S., Danabasoglu, G., Large, W. G., and McWilliams, J. C.: Mechanisms governing interannual variability of upper-ocean temperature in a global hindcast simulation, J. Phys. Oceanogr., 37(7), 1918–1938, 2007.

20 Falcini, F., Iudicone, D., and Salusti, E.: Potential vorticity estimates of absolute velocities on the Ross Sea shelf, Deep-Sea Res. Pt. I, 56, 314–329, 2009.

Farneti, R. and Vallis, G. K.: Mechanisms of interdecadal climate variability and the role of ocean-atmosphere coupling, Clim. Dynam., 36, 1, 289–308, doi:10.1007/s00382-009-0674-9, 14 October 2009.

25 Gent, P. R. and McWilliams, J. C.: Isopycnal mixing in ocean circulation models, J. Phys. Oceanogr., 20, 150–155, 1990.

Gill, A. E.: Atmosphere-Ocean dynamics. Academic Press, NY, 662 pp., 1982.

Haarsma, R. J., Selten, F. M., and Opsteegh, J. D.: On the mechanism of the Antarctic Circumpolar Wave, J. Climate, 13(9), 1461–1480, 2000.

30 Hasselmann, K.: Stochastic climate models, part I: theory, Tellus, 28, 473–485, 1976.

Hogg, A. M. and Blundell, J. R.: Interdecadal variability of the Southern Ocean, J. Phys. Oceanogr., 36(8), 1626–1645, 2006.

Hogg, A. M., Dewar, W. K., Killworth, P. D., and Blundell, J. R.: A Quasi-Geostrophic Coupled Model (Q-GCM), Mon. Weather Rev., 10, 2261–2278, 2003.

Hughes, C. W., Meredith, M. P., and Heywood, K.: Wind-driven transport fluctuations through Drake Passage: a Southern Mode, J. Phys. Oceanogr., 29(8), 1971–1992, 1999.

Jacobs, G. A. and Mitchell, J. L.: Ocean circulation variations associated with the Antarctic Circumpolar Wave, Geophys. Res. Lett., 23(21), 2947–2950, 1996.

James, I. N. and James, P. M.: Spatial structure of ultra-low frequency variability of the flow in a simple atmospheric circulation model, Q. J. Roy. Meteorol. Soc., 118, 1211–1233, 1992.

Levitus, S. and Boyer, T. P. : World ocean atlas 1994. US Department of Commerse, NOAA, NESDIS, Washington DC, 1994.

Liu, W. T., Katsaros, K. B., und Businger, J. A.: Bulk parametrization of air-sea exchanges of heat and water vapor including the molecular constraints at the interface, J. Atmos. Sci., 36, 1722–1735, 1979.

Mantua, N. J. und Hare, S. R.: The Pacific Decadal Oscillation, J. Oceanography, 58, 35–44, 2002.

Marsland, S. J., Latif, M., and Legutke, S.: Antarctic circumpolar modes in a coupled ocean–atmosphere model, Ocean Dynam., 53, 323–331, doi:10.1007/s10236-003-0041-z, 2003.

Mikolajewicz, U., Sein, D. V., Jacob, D., Königk, T., Podzun, R., and Semmler, T.: Simulating Arctic sea ice variability with a coupled regional atmosphere-ocean-sea ice model, Meteorol. Z., 14(6), 793–800, 2005.

Nigam, S., Chung, C., and DeWeaver, E.: ENSO diabatic heating in ECMWF and NCEP-NCAR reanalysis, and NCAR CCM3 simulation, J. Climate, 13(17), 3152–3171, 2000.

Olbers, D. and Eden, C.: A simplified general circulation model for a baroclinic ocean with topography. Part I: theory, waves and wind-driven circulations, J. Phys. Oceanogr., 33, 2719–2737, 2003.

Olbers, D. and Lettmann, K.: Barotropic and baroclinic processes in the transport variability of the Antarctic Circumpolar Current, Ocean Dyn. 57, 559–578, doi:10.1007/s10236-007-0126-1, 2007.

Olbers, D., Lettmann, K., and Timmermann, R.: Six circumpolar currents – on the forcing of the Antarctic Circumpolar Current by wind and mixing, Ocean Dynam., 57, 12–31, doi:10.1007/s10236-006-0087-9, 2007.

Opsteegh, J. D., Haarsma, R. J., Selten, F. M., and Kattenberg, A.: ECBILT: a dynamic alternative to mixed boundary conditions in ocean models, Tellus, 50A(3), 348–367, 1998.

Simulating Southern Hemisphere extra-tropical climate

H. Kurzke et al.

Pacanowski, R. C.: MOM 2 Version 2.0 (*Beta*) Documentation User's Guide and Reference Manuel, GFDL Ocean Technical Report 3.2. 329 pp, 1996.

Pacanowski, R. C. and Griffies, S. M.: MOM 3.0 Manuel, NOAA/Geophysical Fluid Dynamics Laboratory, Princeton, USA 08542., 680 pp., 2000.

5 Roebber, P. J.: Climate variability in a low-order coupled atmosphere-ocean model, Tellus, 47A, 473–494, 1995.

Sarkisyan, A. S. and Ivanov, V. F.: Joint effect of baroclinicity and bottom relief as an important factor in the dynamics of sea currents, Akad. Nauk Atmos. Oceanic Phys., 7(2), 173–188, 1971.

10 Sempf, M., Dethloff, K., Handorf, D., and Kurgansky, M. V.: Idealized modeling of the northern annular mode: orographic and thermal impacts, Atmos. Sci. Lett., 6, 140–144, doi:10.1002/asl.106, 2005.

Sempf, M., Dethloff, K., Handorf, D., and Kurgansky, M. V.: Towards understanding the dynamical origin of atmospheric regime behavior in a baroclinic model, J. Atmos. Sci., 64, 887–904,

15 2007a.

Sempf, M., Dethloff, K., Handorf, D., and Kurgansky, M. V.: Circulation regimes due to attractor merging in atmospheric models, J. Atmos. Sci., 64, 2029–2044, 2007b.

Thompson, D. W. J. and Wallace, J. M.: Annular modes in the extratropical circulation. Part I: month-to-month variability, J. Climate, 13(5), 1000–1016, 2000.

20 Vallis, G. K.: Mechanisms of climate variability from years to decades, in: Stochastic Physics and Climate Modelling, edited by: Palmer, T. and Williams, P., Cambridge University Press, Cambridge, 2010.

White, W. B. and Peterson, R. G.: An Antarctic circumpolar wave in surface pressure, wind, temperature and sea-ice extent, Nature, 380, 699–702, 1996.

25 Weisheimer, A., Kurgansky, M. V., Dethloff, K., and Handorf, D.: Extra-tropical low-frequency variability in a three-level quasi-geostrophic atmospheric model with different spectral resolution, J. Geophys. Res., 108(D5), 4171, doi:10.1029/2001JD001282, 2003.

Simulating Southern Hemisphere extra-tropical climate

H. Kurzke et al.

(a)   (b)   (c)
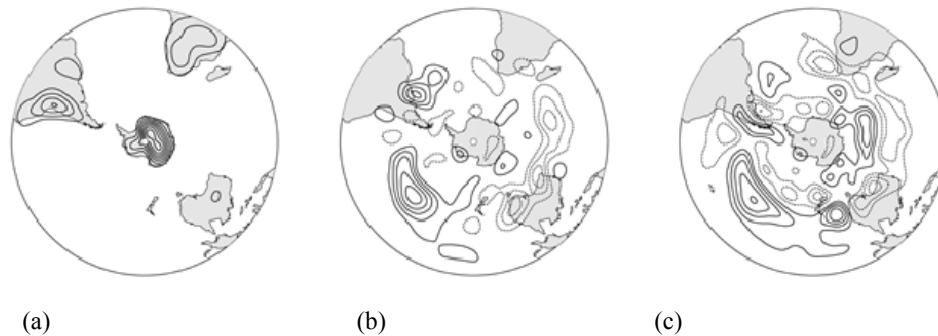
Fig. 1. (a) T21 topography of the Southern Hemisphere. Contour interval is 500 m. **(b)** Non-zonal part of austral wintertime (JJA) extra-tropical diabatic heating at 300 hPa derived from NCEP-NCAR reanalysis data and used in the atmospheric module. Contour interval is 0.25 K day^{-1} without zero line. Negative values are dashed. **(c)** The same as in the middle, but for 700 hPa.

Title Page

Abstract   Introduction

Conclusions   References

Tables   Figures

|◄   ►|

◄   ►

Back   Close

Full Screen / Esc

Printer-friendly Version

Interactive Discussion
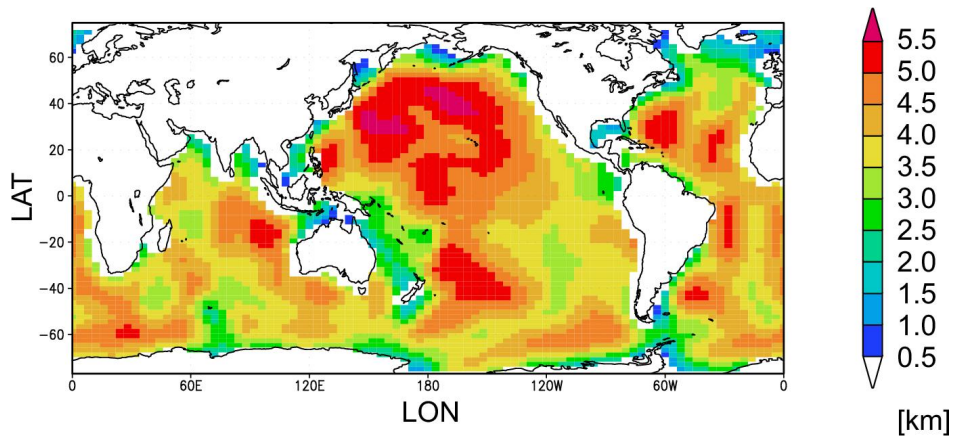
Fig. 2. Bottom topography of the Oceans with realistic coast lines (black contour). Zero bottom isohyps is omitted. Contour (colour) interval is 500 m.
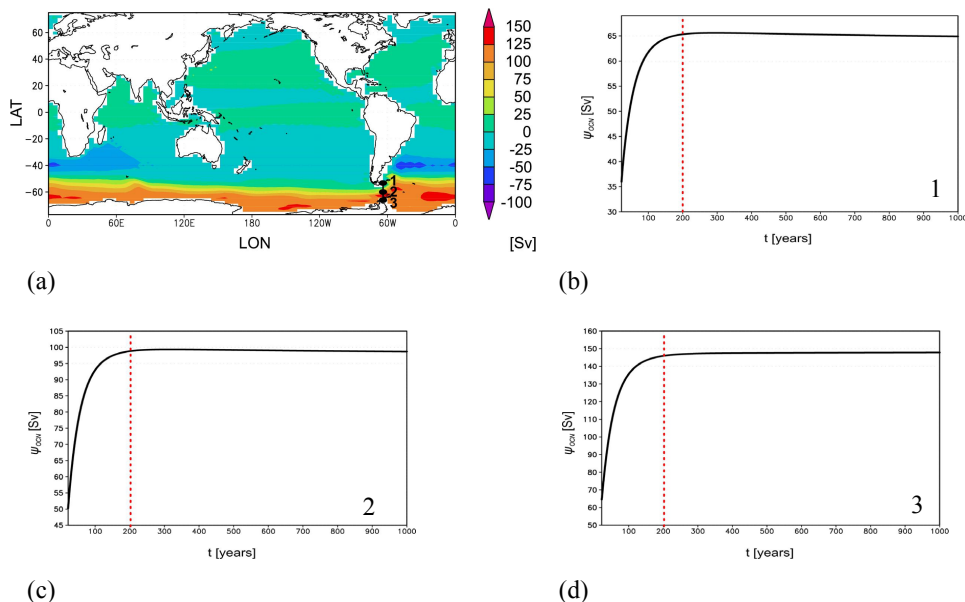
Fig. 3. **(a)** Time-mean of the streamfunction Ψ in Sverdrups ($1\,\mathrm{Sv}=10^6\,\mathrm{m}^3\,\mathrm{s}^{-1}$) over years 190–200 of the uncoupled BARBI model run. Numbers 1, 2, 3 mark the grid points in the Drake Passage, for which a transient behavior of Ψ is shown in **(b)**–**(d)**. **(b)** Ψ-values (Sv) for the grid point with coordinates 59° S and 91° W (point 1 in **a**) versus time in years. **(c)** The same as in **(b)** but for 61° S (point 2 in **a**). **(d)** The same as in **(b)** and **(c)** but for 63° S (point 3 in **a**).
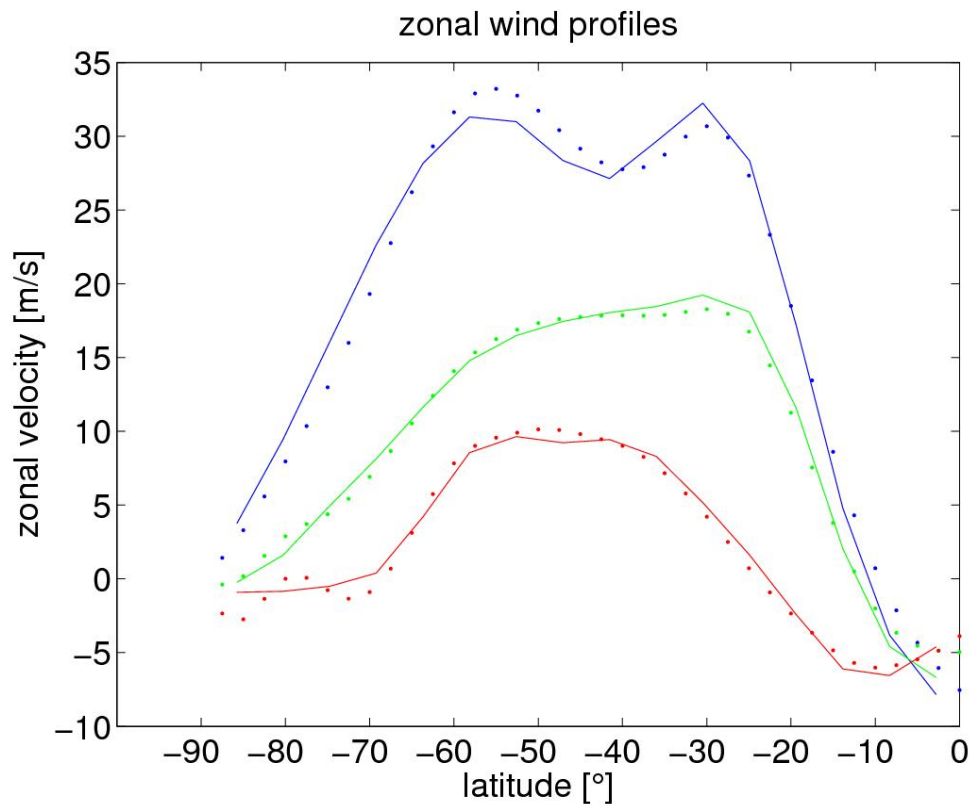
Fig. 4. Modeled (continuous) and observed (dashed) time-mean zonal wind profiles for the three model levels and corresponding vertical layers, respectively.
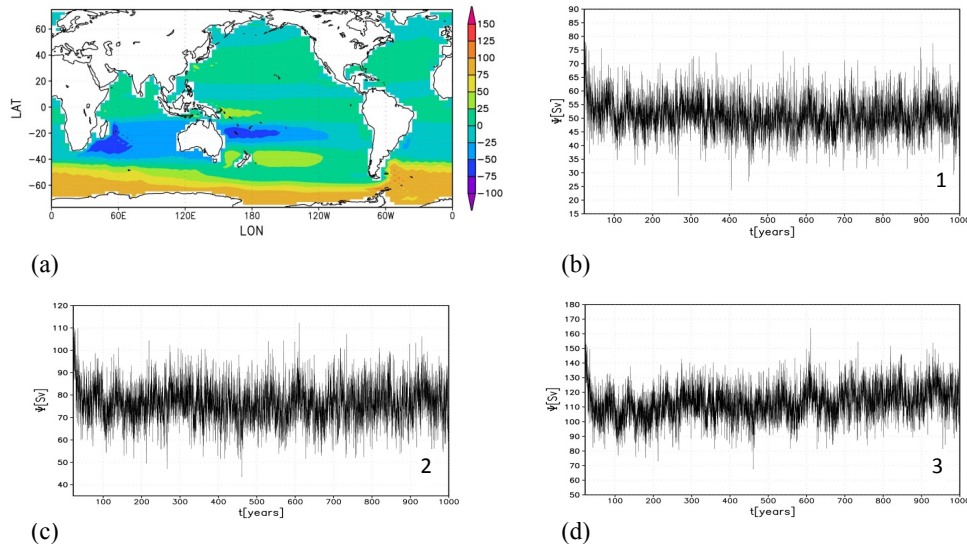
Fig. 5. **(a)** Time-mean of the streamfunction Ψ (in Sv) over last 10 yr the coupled atmosphere-ocean model run. Similar to Fig. 3, numbers 1, 2, 3 mark the grid points in the Drake Passage for which a transient behavior of Ψ is shown. **(b)** Ψ-values (Sv) for the grid point with coordinates 59° S and 91° W (point 1 in **a**) versus time in years. **(c)** The same as in **(b)** but for 61° S (point 2 in **a**). **(d)** The same as in **(b)** and **(c)** but for 63° S (point 3 in **a**).

(a) (b) (c)
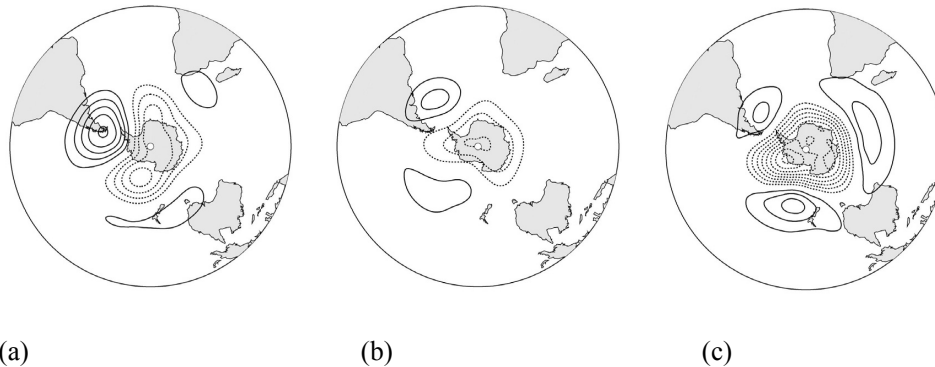
Fig. 6. (a) First EOF of 833 hPa geopotential height for the 1000 yr run of the atmosphere-only model (6.4 % of explained variance). **(b)** First EOF of 833 hPa geopotential height for the 1000 yr run of the coupled model (5.1 % of explained variance). **(c)** First EOF of observed austral wintertime geopotential height in the lowest model level (NCEP-NCAR reanalysis data for 1948–2003) (14.6 % of explained variance).
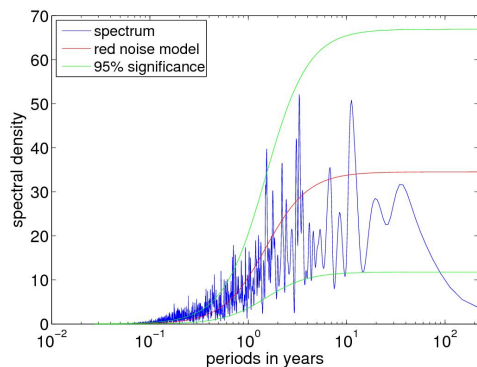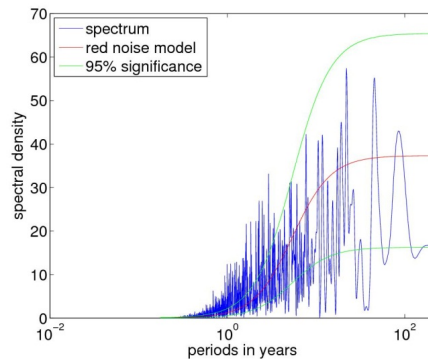
Fig. 7. (a) Power spectrum of PC 1 for the atmosphere-only model 1000 yr run. **(b)** The same as in **(a)** but for the coupled model 1000 yr run.

Full Screen / Esc

Printer-friendly Version

Interactive Discussion
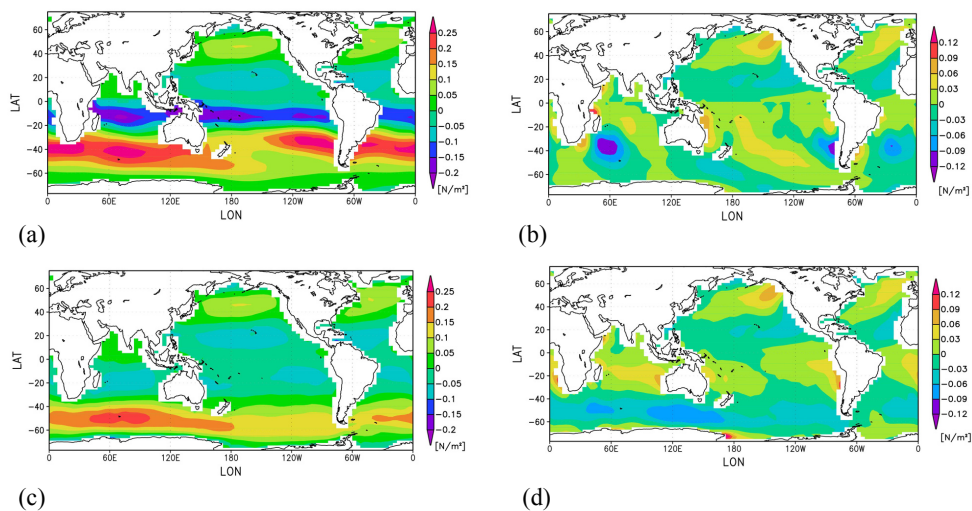
Fig. 8. (a) 1000 yr mean climatology of τ_x (N m^{-2}) for the coupled model run. **(b)** The same as in **(a)** but for τ_y (N m^{-2}) **(c)** The same as in **(a)** but for the ocean-only model run. **(d)** The same as in **(b)** but for the ocean-only model run.

Full Screen / Esc

Printer-friendly Version

Interactive Discussion

(a)   (b)
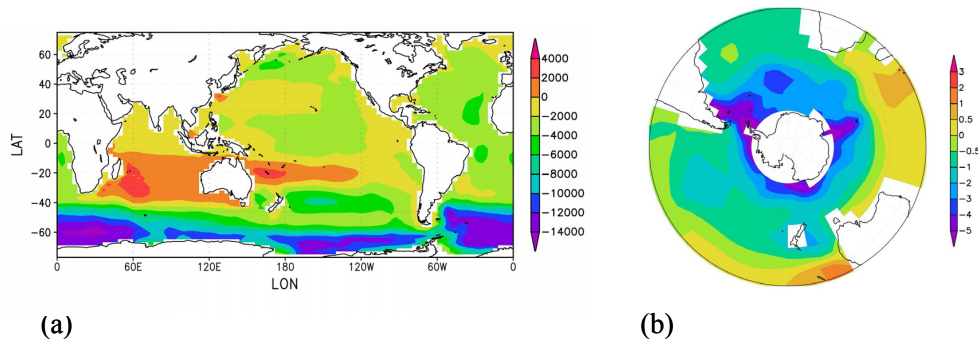
Fig. 9. (a) 1000 yr mean climatology of $E\,(\mathrm{m}^3\,\mathrm{s}^{-2})$. **(b)** The same as in **(a)** but for SST' over the Southern Hemisphere (K).
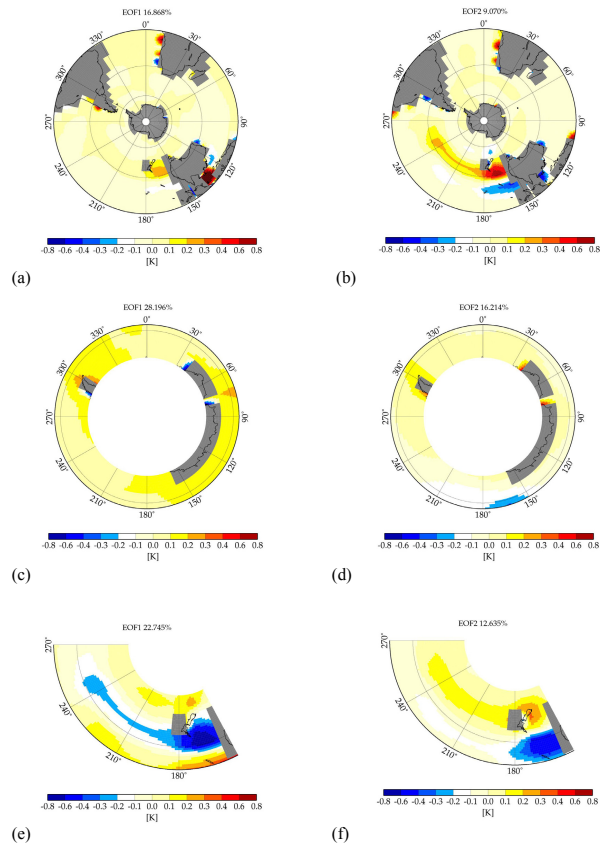
Fig. 10. (a) First EOF of *SST′* over the Southern Hemisphere. **(b)** The same as in **(a)** but for the second EOF. **(c)** The same as in **(a)** but over the ACC (60˚–70˚ S). **(d)** The same as in **(c)** but for the second EOF. (e) The same as in **(a)** but for the Southern Pacific region (20˚–60˚ S, 152˚ E–90˚ W). **(f)** The same as in **(e)** but for the second EOF.
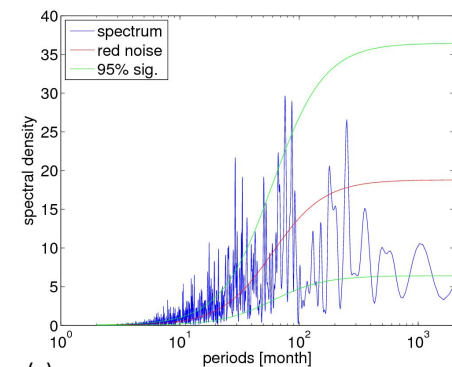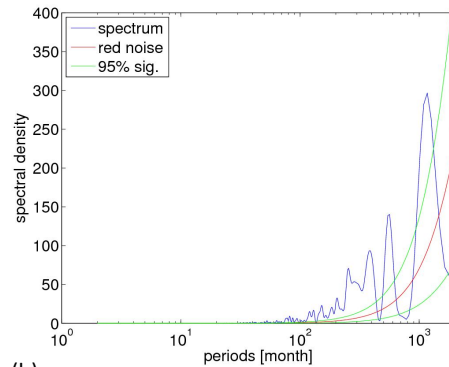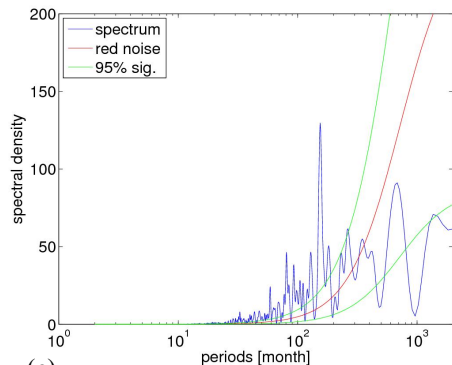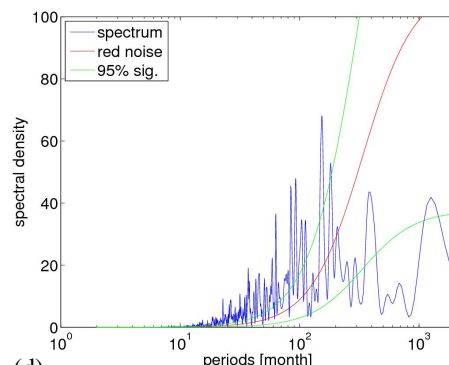
Fig. 11. **(a)** Power spectrum for the monthly-averaged PC1 of the geopotential height at 833 hPa model level for 1000 yr run. **(b)** The same as in **(a)** but for SST' over the ACC. **(c)** The same as in **(b)** but for PC2. **(d)** The same as in **(b)** but for the Southern Pacific.
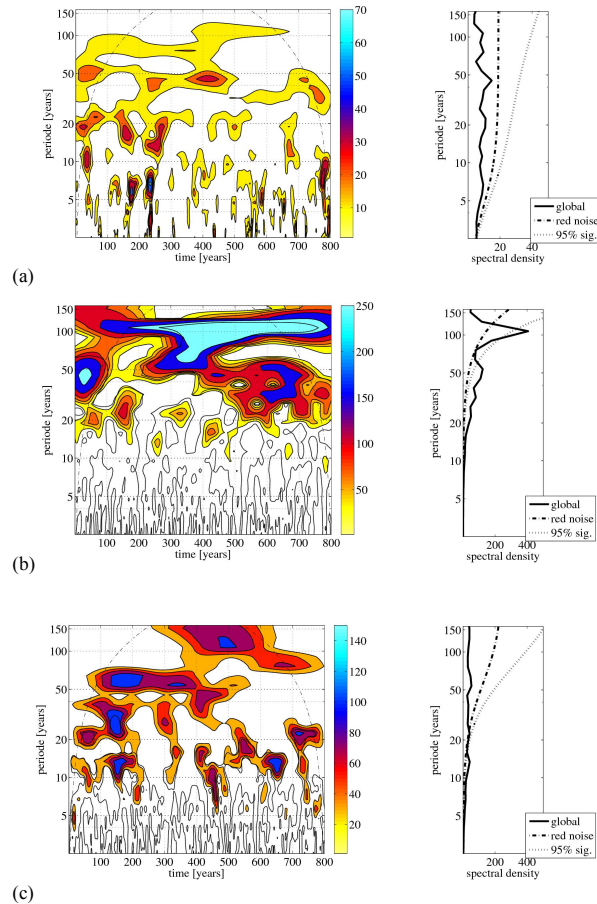
Fig. 12. (a) Wavelet spectrum for the monthly-averaged PC1 of the geopotential height at 833 hPa model level for 1000 yr run. **(b)** The same as in **(a)** but for *SST′* over the ACC. **(c)** The same as in **(b)** but for PC2.